IX. THERMIONICS

Roland Breitwieser and Herman Schwartz

INTRODUCTION

The state of art of several aspects of thermionics as it is considered in the framework of a space power system is reviewed herein. NASA contractual and in-house efforts are emphasized. The principle of thermionics is discussed, and a brief exposure to some pertinent characteristics of thermionic converter systems is introduced. Primary emphasis is placed on (1) establishing the major performance constraints based on fundamental surface and plasma physics, (2) illustrating empirical performance, (3) introducing a few reactor-converter interface considerations, and finally (4) reviewing some limitations of prospective thermionic nuclear reactor fuels. It should be noted, since the NASA sponsored work is stressed, that many excellent references relating to these subject areas have been excluded from this report.

EFFICIENCY CONSIDERATIONS AND THERMIONIC REACTOR SYSTEMS

Figure IX-1 illustrates the basic principle of thermionic conversion. The converter is simply two metal electrodes separated by a small gap. Heat is applied to one metal electrode from an energy source such as a nuclear fuel. As the metal temperature increases, electrons are boiled out and are captured on the cooler electrode. The emission and capture of electrons provide the current flow through the external load. The voltage that can be obtained is depicted in the potential diagram. The hotter electrode, the emitter, has a relatively large population of electrons in the higher energy levels compared with the cooler electrode, the collector. The variation in the electron density is the driving force that permits the development of a useful voltage. Characteristically this is about 3/4 volt. The thermionic converter is a unique heat engine since it is one of the few energy conversion methods that produces electric power directly from heat over a large temperature interval in a single step. It is also unique in its ideal efficiency. A simplified expression for the efficiency is

$$\eta_{el} = \frac{J_{net}(V_1 - V_2)}{J_{net}V_1} \approx \eta_{Carnot} \qquad (V_1 >> kT) \tag{1}$$

where the output term, electric power, is the net current times the difference in the emitter and collector voltage barriers. The input term is simply the energy involved in elevating the elec-

trons to the higher energy levels so that the current can flow over the potential barrier. If the potential barrier is large in comparison with the kinetic energy of the electrons in transit, and if the barriers V_1 and V_2 are adjusted to match the absolute temperature ratio, the Carnot cycle efficiency is approached. These highly idealized conditions neglect the ever-present loss terms. Figure IX-2 removes us from this never-never land of ideality into the reality of the actual thermionic device.

The dictates of the energy source require high power densities, thus, high current densities. At the present time, the high current densities require high emitter temperatures to produce the necessary flow of electrons. In order to sustain the high current densities, a partially ionized gas must be introduced into the interelectrode space. Electron scattering then exists. Radiation transport becomes significant because of the large temperature difference. Gaseous thermal conduction in the interelectrode space also results. Ion flow negates some of the electron current and also transports energy. In order to extract the electric power, leads must be attached to the hot and cold electrodes. Excessive heat is conducted if the lead is too big, or excessive voltage losses if the lead is too small.

The expression for efficiency departs from the Carnot-like expression of equation (1) to the practical expression of efficiency of equation (2):

$$\eta_{el} = \frac{(J_{net})(V_1 - V_2 - \Delta V)}{J_1(V_1 + 2kT_1) - J_2(V_1 + 2kT_2) + \Sigma\dot{Q}} \neq \eta_{Carnot} \qquad (2)$$

The difference between the expressions in the numerator involves a voltage drop and a correction to the net current that accounts for electrical leakages. The denominator increases because of the need to recognize kinetic energy of the electrons and the summation of the many losses enumerated above.

The highly optimistic approach, in which only the first-order constraints of the various physical constants of the materials available to thermionics are used, predicts an efficiency somewhere between one-half and two-thirds of the Carnot-cycle efficiency. In practice, because of some yet inescapable plasma voltage losses, practical converters are achieving only a bit over one-third of the Carnot-cycle efficiency. Even though the present-day fraction of Carnot efficiencies of thermionic energy conversion are not amongst the highest, certain features of thermionics are attracting interest for the potential application to a nuclear energy source, particularly for space application.

Some of these qualities are illustrated in the next few figures. An elaborate nuclear thermionic design is not illustrated. Instead a simplified design has been selected, mainly to demonstrate the basic principles and problems of in-pile nuclear thermionics. However, some of the details of the converter element design do employ practices found useful in research converters. The three main parts of the system are reactor, shield, and radiator (fig. IX-3). The radiator is considerably smaller than other space power systems, since the operating temperatures are higher. Segmented radiators coupled with similar segmented reactor elements are suggested. Each one of the reactor segments is further subdivided into unit thermionic cells (fig. IX-4). The cells are mounted in a tray and are cooled by liquid metal flowing across the tray similar to the

usual crossflow heat exchanger. The arrangement shown has two cells connected in series in each cylindrical station. Each double converter module should develop about $1\frac{1}{2}$ volts. Conceptually, one can visualize the thermionic reactor as a group of $1\frac{1}{2}$ volt batteries connected in some series, parallel network to provide both the necessary voltage and current and to provide reliability through redundant cross connections.

The detail of an individual cell is shown in figure IX-5. Nuclear fuel such as uranium dioxide is introduced in the center. A vented fuel capsule is shown. The encapsulated fuel is electrically isolated by an insulator. The fuel cladding then serves as an electron emitter. The electrons flow to the collector, which is typically a trilayer tube constructed of a thin layer of aluminum oxide sandwiched between layers of niobium. The trilayer tube simultaneously serves as the collector surface, current lead, and heat-exchanger surface. It is cooled by liquid metal as was discussed previously. Cesium gas is introduced into interelectrode space by the use of a cesium reservoir or cesium dispenser material.

The main advantage of the in-pile thermionic conversion system is the high source temperature of this heat engine. The nemesis of most space power is the temperature limit imposed by the liquid-metal corrosion limit and/or the high-temperature strength characteristics of materials. This limitation is avoided by not exposing the liquid metal to the high-temperature source. Instead, the liquid metal is only exposed to the collector, which is at the point of heat rejection. The high-temperature zones can be lightly stressed since the high-temperature surfaces are exposed only to a very low pressure ionized gas. The other attractive feature of this system is the modular design. The modular design offers reliability through redundancy and eases testing problems. The system subdivides into a series of building blocks such as radiators, reactor compartments, and individual cells. Designs like the one illustrated permit out-of-pile testing of the individual cells and groups of cells. The individual thermionic cells can also be introduced into a test reactor for studies of the nucleonic interactions. It has been said that the scaling by multiplicity feature of thermionics permits the development of a power system with a nuclear source that has many of the advantages photovoltaics has provided the solar source. The disadvantages are fairly obvious. The reactor design and fabrication certainly are not simple.

The reactor complexity can be avoided by an alternate approach in which the thermionic converters are external to the reactor, as shown in figure IX-6. A conventional compact liquid-metal-cooled reactor is used. The hot liquid metal is circulated through a thermionic heat exchanger. The heat is rejected through an additional liquid-metal loop to the radiator. Thermionic conversion is achieved in a multipassage heat exchanger. The system illustrated uses an insulated trilayer inner tube that houses the high-temperature liquid metal and also acts as the electron emitter (fig. IX-7). The second trilayer tube houses the ionized gas needed for the converter, serves as a collector, and is sectioned to provide a series of individual thermionic converters. The annulus formed by the outside tube and the second trilayer tube contains the liquid-metal coolant. Many variations of external thermionics exist. This system is not necessarily advocated but merely illustrates some of the more obvious features of external thermionics. The advantages of a simple reactor approach coupled with modular thermionics exist but, unfortunately, the liquid-metal loop is exposed to the reactor fuel temperature. Thus, the system is limited to low source temperatures, a region somewhat unattractive to the electronics of thermionics. Also, from a safety view, if the fuel cladding ruptures, the liquid-metal loop may be con-

taminated with fission products.

If a system analysis is made for either the in-pile or out-of-pile thermionic approach, the performance levels for the converters required to make the system competitive to other power systems becomes established. Roughly, the net power (numerator of eq. (3)) should exceed 5 watts per square centimeter at 2600° F and should exceed 10 watts per square centimeter at 3000° F. The efficiency should approach or exceed 30 percent of the Carnot cycle efficiency, as shown in equation (3):

$$\eta_{el,\,av} = \frac{(J_{net})(V_1 - V_2 - \Delta V)}{J_1(V_1 + 2kT_1) - J_2(V_1 + 2kT_2) + \Sigma\dot{Q}} \geqslant 30 \text{ percent of Carnot} \qquad (3)$$

The remainder of this paper treats the probability of achieving the required efficiency indicated in equation (3), the power densities, and the operating life (at the high temperatures involved) from the viewpoint of basic surface and plasma physics, empirical converter performance, reactor interface problems, and thermionic reactor limitations.

SURFACE PHYSICS

The physics of thermionic energy conversion reduce to the problem of getting the electrons out of the emitter, across the interelectrode gap, and into the collector efficiently. Figure IX-8 shows the problem of getting the electrons out of the emitter. The high temperatures involved in thermionics require the use of refractory metals. Unfortunately, the same interatomic forces that hold a metal together also bind the electrons to the surface. This electron affinity is described quantitatively by the electron work function, which is so named because the term expresses the work required to extract an electron from the surface. The electron emission rate equation, $J = 120T^2 \exp - \varphi/kT$ ampere per square centimeter, is the Richardson-Dushman equation. Using a typical work function for tungsten and plugging in a temperature of 1923° K (3000° F) results in an emission current density of only 0.4 milliampere. Therefore, the work function must be lowered to provide for more emission. This is achieved usually by depositing a partial layer of a low work function metal over the surface of the refractory emitter. Practical thermionic converters usually use cesium. The low work function layer is maintained by continuously flooding the emitter surface with cesium gas.

An interesting and fortunate characteristic of the adsorption process is that the higher the work function, the more refractory the metal, the stronger the cesium attachment to the surface (refs. 1 and 2). An experimental correlation recently noted by the Field Emission Corporation (ref. 3) illustrates this effect (fig. IX-9). The bare work function, that is, the metallic surface, free of any adsorbed particles is the abscissa. The maximum change in work function that can be produced by adsorbing cesium on the surface is given in the upper ordinant. The change in work function overcompensates for the initial high value of the substrate, so that the lowest value of work functions of cesiated surface are achieved with the surfaces that have the highest initial bare work function. The field emission experiments used in obtaining these data permitted

the identification of individual crystal planes. It was noticed that this correlation held for individual crystal index planes of the same metal, and indeed a tungsten surface, oriented to expose a 110 Miller index plane, is one of the more desirable surfaces for the cesium adsorption and retention process. This field emission study and other similar research (refs. 1, 2, and 4) indicate that high work functions are desired not only for the minimum work function but at the intermediate work function values used in practical thermionic converters.

Some idea of the nature of the substrate surface as a function of the crystallographic orientation can be obtained from simple models of the surface. Figure IX-10 shows some of the results of a model based on interaction of a test particle with an array of substrate atoms arranged to give a particular surface orientation (ref. 5). Two surfaces of a body-centered cubic crystal typical of tungsten, tantalum, and molybdenum are shown. The surfaces treated are a 110 surface that corresponds to a slice through the crystal that intercepts the center atom in the crystal. The 100 plane corresponds to the face of a cubic crystal. If an interaction potential corresponding to an attractive and repulsive force that is inversely proportional to the sixth and twelfth power of the distance between particles, respectively, is assumed to exist between the test particle and all the atoms of the substrate and, if a lattice constant and test particle size of σ/a are chosen to match the surface and adsorbate dimensions, topographical potential plots of the surface can be generated. Each contour line corresponds to a constant adsorption energy. The 110 plot shown is not for the entire surface of a unit cell but only for that fraction outlined by the dashed lines in the crystal. The rest of the pattern is repetitive across the 110 face. From these contour plots, relative surface diffusion barrier heights, relative adsorption energies, and number of adsorption sights can be deduced. Various interactions potentials can be assumed. The 6-12 interaction potential used is a convenient mathematical expression that satisfies many of the physical experimental observations.

The results of this analysis indicates the 110 tungsten plane is of interest to thermionics because it provides a large number of adsorption sights with relatively strong adsorption energies and, furthermore, should be thermally stable in terms of self-diffusion.

Recent experimental developments permit a detailed examination of the stability of the surface layer. Table IX-1 presents the results of some of these studies of surface layers by the low-energy electron diffraction (LEED) technique (ref. 6 and data obtained by H. E. Farnsworth et al. under NASA Grant NsG 373). Information on the initial surface layer and adjacent sublayers can be obtained by changing the energy of the incident electron and observing the intensity of the diffracted beam pattern. Several monocrystals of tantalum, molybdenum, and tungsten have been examined. The crystals were cut so that the 110 and 130 Miller index planes were parallel to the surface. Several temporary surface structures were produced on these crystals. The 130 and 310 surfaces on the tantalum were developed by ion bombardment. The 130 surface of molybdenum was produced by cutting followed with appropriate surface treatment. The 110 surface of molybdenum appeared naturally after heating because of the substrate orientation. The tungsten sample was ion bombarded, and a random surface orientation resulted. The crystals that had a bulk orientation of 110 reoriented to a 110 surface after thermal annealing in vacuum at temperatures close to those experienced in a practical thermionic converter. The molybdenum sample with a 110 bulk orientation maintained a 110 orientation through to the surface even after extensive heat treatment. The crystal with a 130 bulk orientation relaxed

back to the 100 and 110 surface planes as would be expected from free-energy considerations of the surface and crystal. Therefore, it appears that the 110 oriented surface can be produced and maintained in vacuum if the bulk orientation is 110. Although these encouraging results can be obtained from small zoned refined monocrystalline samples, the question remains can we reduce this approach to actual practice? For example, can the oriented surfaces be established on the surface of a cylinder?

Recently developments in tungsten fabrication by vapor phase deposition of tungsten is one approach that is quite promising in this regard. Tubes such as shown in figure IX-11 have been routinely, though not always reproducibly, fabricated by vapor deposition. The vapor-deposited tubes are near theoretical density, leak tight, exhibit good structural properties, and, if required, can be deposited in quite complex shapes. The vapor deposition involves hydrogen reduction of a tungsten halide on the heated mandrel. It has been observed that if tungsten hexachloride is used, the bulk sample exhibits a strong 110 orientation parallel to the surface of the mandrel. For tungsten hexafluoride, a 100 bulk orientation results. Photomicrographs (obtained by L. Yang, General Atomic Div. General Dynamics Corp., under NASA Contract NAS 3-8504) of the chloride and fluoride tungsten products after heat treatments are shown in the lower part of figure IX-11. The tungsten hexafluoride samples with their small columnar grain structures should exhibit superior mechanical properties except that the noninterrupted columnar grain boundaries that propagate through the metal may enhance mass diffusion, as will be discussed later in this paper. A series of preliminary tests were performed on a group of vapor-deposited disks (ref. 7) to see if the bulk orientation affected the surface orientation in the same manner as observed in the small zone refined monocrystalline studies (table IX-2). The surface was characterized in terms of the thermionic emission work function. The vapor-deposited tungsten surfaces produced by careful grinding, polishing, and thermal treatment reflected the bulk orientation as determined by work function measurement. Consistently the tungsten fluoride product samples of the 100 orientation gave the lower work functions than the samples with a 110 bulk orientation. A series of surface treatments was made on samples, including additional thermal treatment, chemical etch and electrochemical etch. The various treatments changed the surface work function but, after high-temperature thermal treatment, all samples relaxed back to the initial work function with the exception of one. Thus, the results on practical surfaces were consistent with the LEED studies. The duplex sample was a single exploratory test to determine if the desirable structural properties of the fluoride product could be combined with the desired surface properties of the chloride product. Some hope exists, for this approach, as evidenced by the high surface work function.

It is assumed herein that the desired thermionic emitter possesses a high substrate work function because of the consistent observations that better cesium adsorption properties result with the high substrate work functions.

Additional adsorption studies are being conducted as part of the NASA thermionic program. The analytical work includes calculations of the binding energies of various adsorbates (refs. 5, 8, 9, and 10), two-species adsorption theory (ref. 11)(e.g., tungsten on cesium), and multiple-species adsorption, where the adsorption of cesium, barium, or strontium on oxidized and fluorided surfaces has been analyzed (refs. 12 to 14). Experimentally, adsorption has been studied by field emission, as was shown in figure IX-9. Molecular beams of cesium, oxygen,

and fluorine have also been utilized to examine the details of dual-species (ref. 15) and multi-species (ref. 16) adsorption. It is interesting to note that oxidizing or fluoriding the surface of refractory metals tends to increase work functions which, in turn, improve cesium adsorption characteristics. The observation that high substrate work functions improve cesium adsorption is again verified even for complex surfaces, a point noted in the development of photoemissive surfaces many years ago. Reproducibility of the additive studies of oxygen and fluorine in the high-temperature, high-current conditions found in thermionic converters is extremely difficult to obtain, however.

The final evaluation still resides in tests in the actual environment of the thermionic converter. Figure IX-12 illustrates experimental results of the now well-documented tungsten-cesium adsorption system obtained in a research-type thermionic converter. A tungsten emitter whose bulk orientation is basically 110 was used. Current density is plotted as a function of cesium pressure. The curves presented for two emitter temperatures are based on experimental data and are fared through the use of an analytical expression (unpublished data of R. Breitwieser of Lewis Research Center). Current densities as high as 100 amperes per square centimeter have been observed by pulse measurements at the higher cesium pressures.

PLASMA CONSIDERATIONS

The unambiguous demonstration of the stability of a 110 tungsten surface at high-temperature, high-current conditions has not been established. It has been verified, however, that more than adequate emission currents are available in a diode if the cesium pressure is sufficiently high. In terms of relative particle flux, it is interesting to note that, at the high-current conditions, 3 to 6 cesium atoms must arrive at the surface per unit time for every electron that is emitted from the same surface. Spacings in a converter, therefore, must be small to avoid electron-atom scattering. Methods exist for getting electrons out of the emitter. The problem remains, however, of getting electrons across the interelectrode space. Figure IX-13 illustrates some of the problems in getting electrons across, and the following outline presents part of the associated research program:

Space charge:

(1) Application of Langmuir theory to electrons and ions

(2) Two-species theory

  (a) Ion and electron current - voltage curves

  (b) Stability analysis

Elastic scattering including space charge:

(1) Isotropic collisions

(2) Energy-dependent and angular-dependent collisions

Cross section:

(1) Atom-atom

(2) Atom-ion

(3) Atom-electron

If no ions are present in the interelectrode space, a large space-charge barrier develops, so that the electron flow is reduced to a mere trickle. For example, an emitter that has an emission capability of over 100 amperes per square centimeter will have all but 1 milliampere of its

current reflected back to the emitter by the space-charge barrier if the interelectrode space is 1 millimeter, if no ions are present, and if the acceleration potential across the surfaces is restricted to 1/2 volt. Ions formed at the surface will reduce the space-charge barrier but, with the exception of thermionic converters which use very high source temperatures, the rate of surface ionization does not produce enough ions to permit the transfer of significant electron currents. The surface ion formation mechanism is now quite well understood (ref. 17), as are the modifications to the space-charge theory which include ions as well as electrons. The ion and electron transport is understood for steady-state conditions (refs. 18 and 19) and in terms of transient stability analyses (ref. 20).

The transmission of a substantial fraction of the emitted current requires that ions be produced in the interelectrode space. It follows, therefore, that some of the energy of the emitted electrons must be diverted to produce the ions. A voltage drop results because of both elastic and inelastic electron scattering. The elastic scattering randomizes the directed velocity of the electron, whereas the inelastic collisions absorb energy of the incoming electron by the excitation or ionization of the target atoms. The elastic scattering process is at a reasonable level of understanding. A new technique exists by which the complexity of the simultaneous effects of space charge, energy-dependent cross sections, and angular-dependent elastic cross sections can be treated to generate theoretical current-voltage curves for thermionic converters (ref. 21 and unpublished data of C. M. Goldstein). A variation of a Monte Carlo transport analysis is used.

As mentioned, experimental and analytic information on the various collision cross sections are being obtained in support of this effort. The atom-atom (ref. 22), atom-ion (refs. 23 and 24), and atom-electron (ref. 24) cross sections are under study. The application of cross section data can be seen in the effect of argon on the elastic scattering of electrons, presented in figure IX-14. Argon exhibits an electron-neutral cross-section minimum in the near-thermal energy range; this effect is called the Ramsauer effect. This strongly energy-dependent cross section provides a stringent analytic exercise when used in electron transport analysis as well as an interesting possible gaseous additive for a thermionic converter. Argon minimizes ion losses by reducing mobility and, thus, wall recombination. Relatively large ion-neutral cross sections compared with the small electron-neutral cross sections in the Ramsauer region provide the needed mechanism.

The current voltage characteristics (in dimensionless units) have been compared with the noncollisional space-charge solution. The collision parameter refers to the product of pressure (in torr) and distance (in cm). These data were calculated by the aforementioned Monte Carlo analytical method (unpublished data of C. M. Goldstein). The slight negative current-voltage slope is caused by the Ramsauer minimum in the energy-dependent cross section. The current reduction of argon is small in comparison with gases such as cesium because of the small cross section in the near thermal range. The analyses in their present forms are merely a first step in the attempt to provide a rigorous, analytical treatment for electron transport that can account for the detailed nature of the electron-neutral collisions and space-charge interactions. As yet, the method has not been used in treating the inelastic portion of the scattering processes although, with additional effort, the approach appears to be completely feasible, although more experimental information on the nature of the emitter sheath would be helpful. Since the details

of getting the electrons across the interelectrode space are not understood as yet because of the yet undetermined inelastic effects, the thermionic field has relied on empirical observations of plasma drops. Lewis results (unpublished data of R. Breitwieser and W. Rush), which are quite consistent with the results of others (ref. 25), indicate that voltage drops of greater than 0.4 volt are always present in the volume ionization mode of practical converters. Voltage drops greater than this minimum exist when the collisional activity is high and can be correlated with the electron-neutral atom collision frequency or, more simply, with the product of gas pressure and interelectrode spacing.

COLLECTOR EFFECTS

Figure IX-15 summarizes a portion of the previous discussion and introduces the problem of getting electrons into the collector. It indicates the approximate type of work function required to achieve the required electron current density from the emitter. The type of plasma sheath and the minimum plasma drop involved in the ignited or volume ionization mode of operation, which involves the aforementioned inelastic collisions, is also in figure IX-15, as well as the type of collector sheath and collector work functions that are needed for the output voltages of a practical thermionic diode. The following collector problems relate first to the confusion of the nature of the collector sheath:

Collector sheath:

- Emission spectroscopy (line shift)
- Laser diagnostics (improved spatial resolution)
- Langmuir probe studies

Adsorption processes:

- Analytical (emphasis on low work function region)
- Experimental (field emission, molecular beam, and diode work)
- Contamination (collector surface "cold" trap impurities)

At times, the ineffectiveness of thermionic conversion is attributed to the collector surface although it is actually because of the properties of the plasma sheath adjacent to the collector. Attempts to strengthen the analysis of the sheath problem are being made by evolving new diagnostic tools that provide the spatial resolution needed to probe the sheath. This first step relates to a definition of the central plasma properties. The line shift method of emission spectroscopy suggests some simplifications in this regard (ref. 26). The laser, with its excellent optical resolution, is being developed as a probe (ref. 27). Recognition of the relation of the refractive index of a plasma to electron density is the principle of the laser plasma probe. Advances in Langmuir probes through miniaturization are being made also (ref. 28). In addition to the problems related to the uncertainties of the sheath at both the collector and emitter, all the adsorption processes must be controlled again to produce the desired collector work function. The emphasis is on a lower work function for the collector. If the allowed operating temperatures, the various potential barrier heights required for the emission of the current densities of interest, and the plasma drops present in the group of converters of the day are considered, the collector work function should be less than 1.8 electron volts to prevent serious in-roads into the output potential of the

devices; for low-temperature thermionics, the lower the better. The adsorption processes are complicated since a single gas pressure exists in the interelectrode space, and it is necessary to attempt to optimize the coverages on both the emitter and collector surfaces with a closely linked arrival rate of the adsorbing species. The inability to achieve low work functions (less than $1\frac{1}{2}$ eV) is one of the contributing reasons for the rapid decay of the performance of thermionics at low operating temperatures. An additional serious collector problem is related to the fact that the collector is the major cool surface in a converter. The collector not only collects electrons, but the various contaminants in the diode as well. The collection of diode debris may seriously affect the adsorption processes, as illustrated in figure IX-15; the debris is represented by the black dots.

The sketch is not pure fiction. Examination of many thermionic converters gives strong visual evidence of collector deposits. The severity of the collector deposits is of course related to the outgassing techniques used in diode preparation, emitter and collector materials, possible nuclear fuel clad interactions, and, in general related to the entire physical-chemical high-temperature stability of the converter assembly.

Diffusion of the nuclear fuel through the emitter clad is a source of collector contamination that has received major attention, since the fuel cladding may not exhibit long-time, high-temperature stability with some of the proposed fuels.

The electron reception characteristics of the collector are affected by extremely small amounts of contamination, since a fraction of an atomic monolayer of contaminant may influence the collector adsorption process. Carefully controlled out-of-pile tests have been used to obtain quantitative information on the rates of diffusion through simulated fueled emitters (table IX-3). The amount of uranium contamination on a cold surface adjacent to a simulated thermionic emitter containing nuclear fuels was measured by either activation analysis or alpha counting. The amount of uranium deposited expressed in terms of equivalent atomic monolayers is shown for 90 mole percent uranium carbide - 10 mole percent zirconium carbide (ref. 30) and uranium dioxide (ref. 31). Two tungsten clads were evaluated for the uranium dioxide. The greatest rate of diffusion was observed for the uranium carbide - zirconium carbide fuel. A possible problem in the use of vapor-deposited tungsten is suggested by the higher rates of uranium diffusion as compared with the powder metallurgy product tungsten. The vapor-deposited tungsten was produced from tungsten hexafluoride and possessed the usual columnar grain structure. The large number of columnar grain boundaries propagating through the clad undoubtedly enhanced fuel diffusion rates. Proper selection of fuel type and cladding promises to minimize the amount of contamination to levels where the use of getters, or natural absorbtion characteristics of collector materials can accommodate low rates of material transport.

CONVERTER PERFORMANCE

Having traced our way across the converter and having established some of the thermionic converter problems, the next few figures deal with the reduction to practice of the aforementioned research. Figure IX-16 shows the latest type of research converter, which is undergoing preliminary orientation tests prior to in-pile- evaluation. The planar configuration was chosen to provide for ease in instrumentation and ease in evaluating new design approaches. The emitter

consists of duplex vapor-deposited tungsten bonded on tantalum. The emitter is essentially identical to the duplex sample referred to in table IX-2. The tungsten formed from the tungsten chloride (WCl_6) is on the outer surface to provide for the beneficial adsorption properties of a high work function material. The inner layer formed from tungsten fluoride (WF_6) is presumed to give better structural properties. The collector is a niobium - niobium alumina cermet - niobium trilayer. The niobium cermet serves as an electrical insulator between the emitter and the collector and as an electrical insulator between the collector and the heat sink. The niobium cermet is only 23 mils thick; thus, it is a good thermal conductor. The cermet is made by hot isostatic pressing of niobium spheres that were precoated with high-purity alumina. The vapor-deposited alumina coatings were graded to provide for an increasing alumina concentration toward the center of the cermet. The dark areas in the photomicrograph in figure IX-16 correspond to the alumina, and the light areas correspond to the niobium. The cold resistance of the cermet is typically greater than 10 megohms for a 1-square-centimeter sample. Initial tests of the diode are in process. The collector properties, in terms of structural reliability, and thermal and electrical characteristics are very encouraging. The emitter has indicated favorable structural stability during the initial series of thermal annealing and degassing processes. To date, cesiated performance has not been obtained.

Figure IX-17 presents results of the electrical performance of converters that reflect the technology of the 1964 - early 1966 time period. Power densities observed at conditions corresponding to maximum efficiency are shown as a function of emitter temperature for the converters. The higher performance corresponds to data obtained in a research-type converter built in late 1965 and early 1966 (obtained by J. Lawrence under NASA Contract NAS 3-8511). The lower performance data, indicated by data points, are typical of converters fabricated about 2 years ago and used in tests evaluating the life of thermionic converters (ref. 32). Tungsten emitters and niobium collectors were used for both groups of converters. Insufficient documentation of the detailed properties of the emitter and collector processing, as well as some questions of data accuracy in the life-test converters, precludes a quantitative explanation of the difference in performance. The performance curve is typical of the carefully processed thermionic converter being tested presently and is a conservative example. Several performance mappings of converters tested during the first half of 1966 indicate even higher performance.

Typical performance values of the research converter are: output voltage at 2000° K is 0.7 volt, efficiency of approximately 15 percent. At the temperature ratios used, the efficiency is about 30 percent of Carnot cycle efficiency. The ability to produce single converters that exhibit useful power levels and efficiencies has been demonstrated. The ability to assemble large groups of high performance diodes, as projected in systems studies, remains to be proven.

The problem of reliable operation has undergone examination in both in-pile and out-of-pile thermionics. Tables IX-4 and IX-5 present typical out-of-pile results. The results (ref. 32) summarized in table IX-4 are from cylindrical diodes electrically heated to 2100° K with a power density of 7 to 11 watts per square centimeter and an efficiency of 12 to 13 percent throughout the tests.

The 300 series diodes used vapor-deposited tungsten emitters supported on tantalum sleeves.

stability on thermal cycling. This characteristic is often present in composite materials of mixed tensile and yield strengths. Uranium dioxide - tungsten cermet specimens clad with tungsten have been thermally cycled by electric heating from room temperature to approximately 2000° K for 100 cycles. Insufficient data have been obtained to correlate cracking with fabrication procedure. Figure IX-21 gives the extent of dimensional change for three specimens (data obtained from Battelle Memorial Institute under NASA Contract NAS 3-4255). One of the nonfractured specimens exhibited less than 1 percent growth but, again, the insufficient experimental statistics exist to define specific fabrication procedures that would ensure dimensional stability.

These results reflect the uncertainties in much of thermionics. No fundamental roadblocks to a successful system development are apparent. There are many individual cases of excellent structural characteristics, fuel stability, and converter performance, which all lead to logical system design and testing concepts. However, the small number of tests and the statistical scatter of results certainly indicate the need for more extensive and more controlled testing of many subparts of this potentially attractive space power system.

REFERENCES

1. Levine, J. D.; and Gyftopoulos, E. P.: Adsorption Physics of Metals Partially Covered by Metallic Particles. III. Equations of State and Electron Emission. Surface Sci., vol. 1, no. 4, 1964, pp. 349-360.

2. Rasor, Ned S.; and Warner, Charles: Correlation of Emission Processes for Adsorbed Alkali Films on Metal Surfaces. J. Appl. Phys., vol. 35, no. 9, Sept. 1964, pp. 2589-2600.

3. Bennette, C. J.; Strayer, R. W.; Swanson, L. W.; and Cooper, E. C.: Behavior of Various Adsorbates on Metal Substrates. Final Rep. (NASA CR-54704), Field Emission Corp., Feb. 18, 1966.

4. Houston, J. M.; and Webster, H. F.: Thermionic Energy Conversion. Advance in Electronics and Electron Physics. Vol. 17. L. Marton and Claire Marton, eds., Academic Press, 1962, pp. 125-206.

5. Bacigalupi, Robert J.; and Neustadter, Harold E.: Dependence of Adsorption Properties on Surface Structure for Body-Centered-Cubic Substrates. NASA TN D-3141, 1965.

6. Boggio, J. E.; and Farnsworth, H. E.: Low-Energy Electron Diffraction and Photoelectric Study of (110) Tantalum as a Function of Ion Bombardment and Heat Treatment. Surface Sci., vol. 1, no. 4, 1964, pp. 399-406.

7. Anon: Studies of Thermionic Materials for Space Power Applications. Rep. No. GA-7244 (NASA CR-72043), General Atomic Div., General Dynamics Corp., July 15, 1966.

8. Neustadter, Harold E.; and Luke, Keung P.: Low-Coverage Heat of Adsorption. I - Alkali Metal Atoms on Tungsten; Atom-Metal Interaction Theories. NASA TN D-2430, 1964.

9. Neustadter, Harold E.; Luke, Keung P.; and Sheahan, Thomas: Low-Coverage Heat of Adsorption. II - Alkali Metal Atoms on Tungsten; Lennard-Jones Atom-Atom Interaction Theory. NASA TN D-2431, 1964.

10. Neustadter, Harold E.; and Luke, Keung P.: Low-Coverage Heat of Adsorption. III - Alkali Metal Ions on Tungsten; Atom-Metal Interaction Theory. NASA TN D-2460, 1964.

11. Luke, Keung P.; and Smith, John R.: Theoretical Study of Zero-Field Electron Work Function of Metal Immersed in Gas-Direct Application to Cesium Thermionic Diode. NASA TN D-2357, 1964.

12. Tower, Leonard K.: The Erected Dipole Model in the Adsorption of Cesium on Fluorinated Molybdenum. NASA TN D-3223, 1966.

13. Tower, Leonard K.: A Preliminary Analysis of the Process of Desorption of Multiple Additives from Metals. Paper Presented at the IEEE Thermionic Conversion Specialists Conference, San Diego, California, Oct. 25-27, 1965.

14. Tower, Leonard K.: Desorption Kinetics of Multiple Adsorbates - Cesium with Fluorine on Molybdenum and Tungsten. NASA TN D-3596, 1966.

15. Stickney, R. E.; and Bergman, J. G.: Effect of Fluorine and Oxygen on Thermionic Emission from Polycrystalline Tungsten. 26th Annual Conference on Physical Electronics, Massachusetts Institute of Technology, Mar. 21-23, 1966.

16. Stickney, R. E.; and Fehrs, D. L.: Retarding Potential Measurements of the Work Function of Tantalum as a Function of Cesium Coverage. 26th Annual Conference on Physical Electronics, Massachusetts Institute of Technology, Mar. 21-23, 1966.

17. Breitwieser, Roland; and Rush, Wayne: Saha-Langmuir Surface Ionization Relation. Paper Presented at the IEEE Thermionic Conversion Specialists Conference, San Diego, California, Oct. 25-27, 1965.

18. Goldstein, C. M.: Theoretical Current-Voltage Curve in Low-Pressure Cesium Diode for Electron-Rich Emission. J. Appl. Phys., vol. 35, no. 3, pt. 1, Mar. 1964, pp. 728-729.

19. Goldstein, C. M.: Theoretical Current-Voltage Curve in Low-Pressure Cesium Diode for Ion-Rich Emission. Paper Presented at the IEEE Thermionic Conversion Specialists Conference, Gatlinburg, Tennessee, Oct. 7-9, 1963.

20. Burger, P.: Computer Simulation Methods for Plasma Diodes with Collisions. Paper Presented at the IEEE Thermionic Conversion Specialists Conference, San Diego, California, Oct. 25-27, 1965.

21. Goldstein, Charles M.: Monte Carlo Method for the Calculation of Transport Properties in a Low-Density Ionized Gas. NASA TN D-2959, 1965.

22. Sheldon, John W.; and Manista, Eugene J.: Atomic Beam Determination of the Cesium-Cesium Total Scattering Cross Section. NASA TN D-3160, 1965.

23. Sheldon, John W.: Semiclassical Calculation of the Differential Scattering Cross Section with Charge Exchange: Cesium Ions in Cesium Vapor. NASA TN D-2484, 1964.

24. Bullis, R. H.; and Flavin, R. K.: Research on the Collision Probabilities of Electrons and Cesium Ions in Cesium Vapor. Rep. No. A-920057-5 (NASA CR-50301), United Aircraft Corp., May 31, 1963.

25. Kitrilakis, Sotiris: Correlation of Internal Voltage Loss in Optimized Thermionic Converters. A Symposium on High Temperature Conversion - Heat to Electricity, Univ. of Arizona, Feb. 19-21, 1964. Earl W. Phelan, ed., AEC Rep. No. TID-7687, pp. 214-219.

26. Majkowski, R. F.; and Donohue, R. J.: Cesium Plasma Spectroscopy-Electron Number Density Measured by Stark Shift of Spectral Lines. Final Rep. (NASA CR-54997), General Motors Research Lab., Jan. 14, 1966.

27. Verdeyen, J. T.; Cherrington, B. E.; and Fein, M. E.: Investigation of the Basic Processes Occurring in Gaseous Plasmas in Various Charge Density and Energy States. Second Semiannual Prog. Rep., May 1, 1965 thru Oct. 1, 1965, University of Illinois, Gaseous Electronics Lab., 1965.

28. Morris, J. M.: Small Plasma Probes with Guard Rings and Thermocouples. NASA TM X-1294, 1966.

29. Horner, M. H.: Post-Operation Examination of Thermionic Life-Cells. Rep. No. GA-7131, General Atomic Div., General Dynamics Corp.

30. Anon: Studies of Thermionic Materials for Space Power Applications. Rep. No. GA-6860 (NASA CR-54980), General Atomic Div., General Dynamics Corp., May 6. 1966.

31. Kaznoff, A. I.; and Sanderson, M. J.: Diffusion and Interactions in the Urania-Tungsten and Urania-Molybdenum Systems. Paper Presented at the International Conference on Thermionic Electrical Power Generation, London, Sept. 20-25, 1965.

32. Anon: Research Program for the Long Term Testing of Cylindrical Diodes and the Irradiation of Fuel and Insulator. Rep. No. GEST-2049 (NASA CR-54656), General Electric Co., Apr. 18, 1965.

TABLE IX-1. - STABILITY OF MONOCRYSTALLINE SURFACES

(FROM LEED STUDIES, BROWN UNIVERSITY)

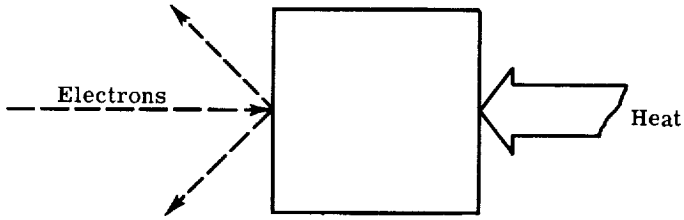

Material	Basic crystal orientation	Initial surface orientation	Surface after heat treatment
Tantalum (BCC)	110	[a]130 and 310	110
Molybdenum (BCC)	130	130	110 and 100
Molybdenum (BCC)	110	110	110
Tungsten (BCC)	110	[a]Random	110

[a]Produced by ion bombardment.

TABLE IX-2. - STABILITY OF VAPOR-DEPOSITED TUNGSTEN SURFACES

(FROM GENERAL ATOMIC)

Process	Initial φ	Etch	Treated φ	Thermal aging		Final φ
				^{o}K	Hr	
Tungsten fluoride (WF_6)	4.52	Thermal	4.52	2073	600	4.52
Tungsten fluoride (WF_6)	4.52	Chemical	4.67	2273 to 2673	18	4.54
Tungsten fluoride (WF_6)	4.51	Electrochemical	4.72	2173 to 2573	36	4.50
Tungsten chloride (WCl_6)	5.01	Thermal	5.01	2073	1040	5.01
Tungsten chloride (WCl_6)	4.93	Chemical	4.85	2673	7	4.94
Tungston chloride (WCl_6)	5.05	Electrochemical	4.89	2173 to 2673	39	4.85
Duplex tungsten chloride - tungsten fluoride (WCl_6-WF_6)	4.86	Thermal	4.86	2073	720	4.86

TABLE IX-3. - URANIUM DIFFUSION THROUGH TUNGSTEN-CLAD EMITTER

[Cladding, 20 mils; test time, 1000 hr.]

Fuel	Temperature		Clad	Number of monolayers
	^{o}K	^{o}F		
90 mole percent uranium carbide - 10 mole percent zirconium carbide	2170	3432	Vapor-deposited tungsten (GA)	230
Uranium dioxide	2100	3320	Vapor-deposited tungsten (GE)	15
Uranium dioxide	2070	3252	Powder metallurgy tungsten	4

TABLE IX-4. - GENERAL ELECTRIC THERMIONIC CONVERTER LIFE TESTS

[Emitter temperature, 2100° K (3320° F); power density, 7 to 11 W/cm^2; efficiency, 12 to 13 percent; electrically heated emitter; percent degradation, none.]

Designation	Duration, hr	Failure mode
301	3754	Emitter support sleeve
302	100	↓
303	916	
311	6413	
312	8055	
313	3775	
431	405	Short
432	151	Short

TABLE IX-5. - GENERAL ATOMIC THERMIONIC

CONVERTER LIFE TESTS

[Emitter temperature, 2000° to 2100° K (3140° to 3320° F); power density, 7 to 9 W/cm^2; efficiency, 11 to 13 percent; electrically heated emitter.]

Designation	Duration, hr	Failure mode	Degradation, percent
LC-1	7 174	Metal-ceramic seal	60
LC-2	3 235	Crack in emitter stem	None
LC-3	10 406	Short	None
LC-4	7 345	Braze joint	None
LC-5	7 558	Braze joint	15
LC-6	2 300	Continuing	[a]40

[a]Low initial power.

TABLE IX-6. - CHARACTERISTICS OF THERMIONIC FUELS

	Uranium carbide	Uranium dioxide	Uranium dioxide - tungsten cermet
Uranium density	High	Medium	Low
Thermal conductivity	High	Low	High
Vapor pressure	Low	High	Not applicable
Probable fission gas management	Release and vent	Release and vent (high temperature)	Retain

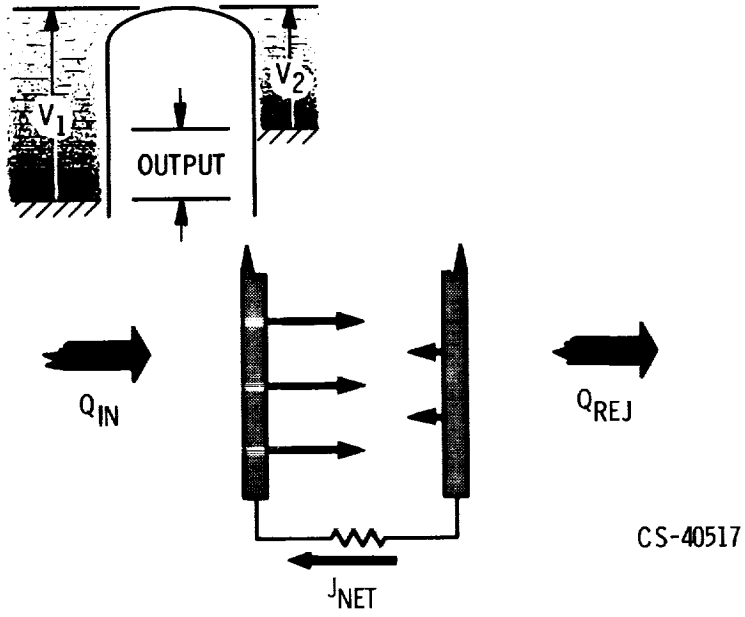

Figure IX-1. - Ideal thermionics.

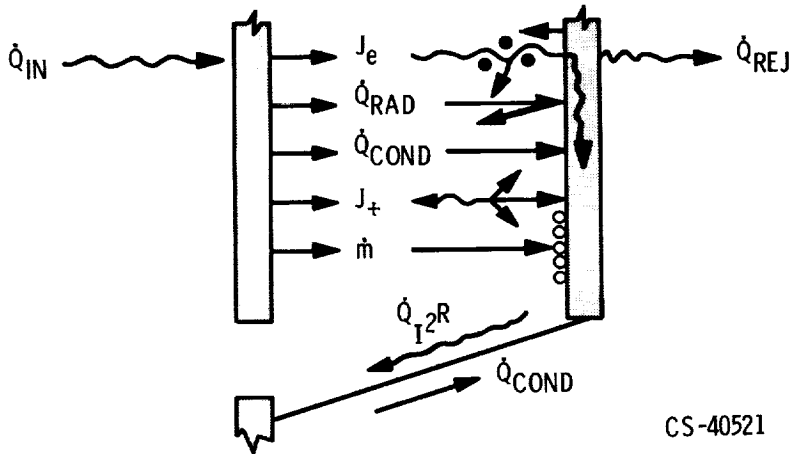

Figure IX-2. - Actual thermionics.

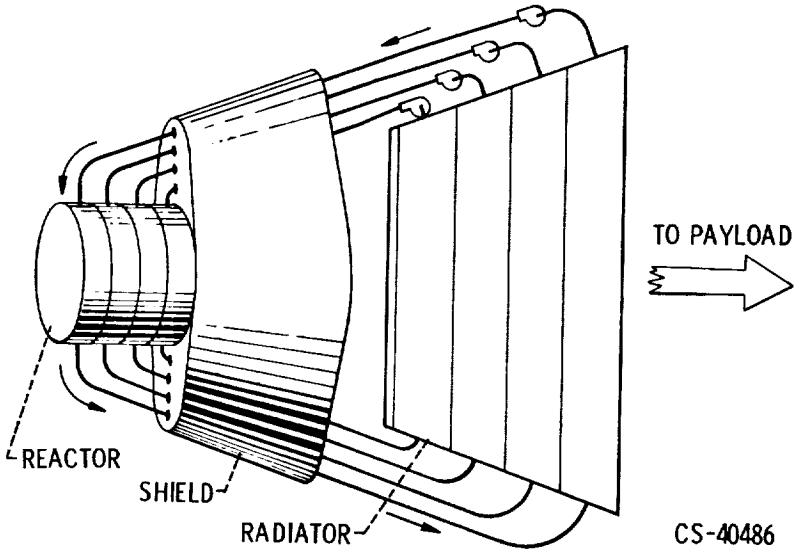

Figure IX-3. - In-pile thermionic system.

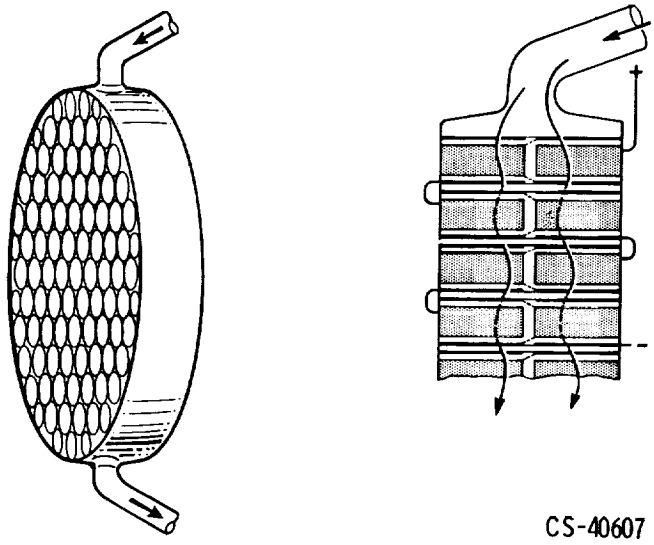

Figure IX-4. - In-pile thermionics crossflow heat exchanger.

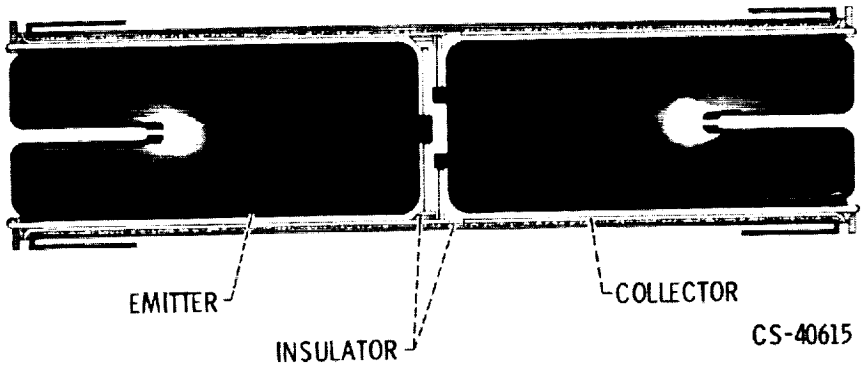

Figure IX-5. - In-pile thermionics unit cells.

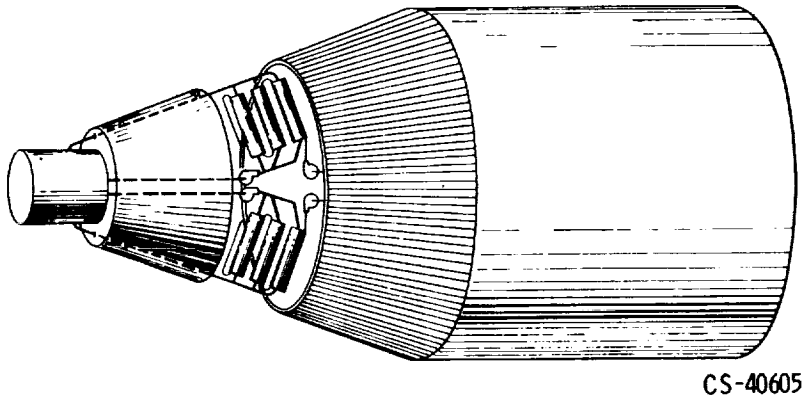

Figure IX-6. - Out-of-pile thermionic system.

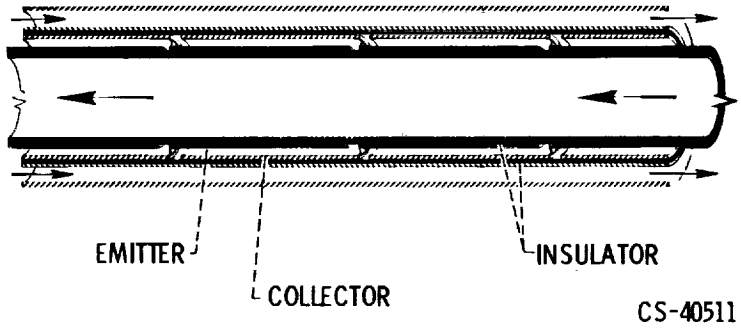

Figure IX-7. - Out-of-pile thermionic converter.

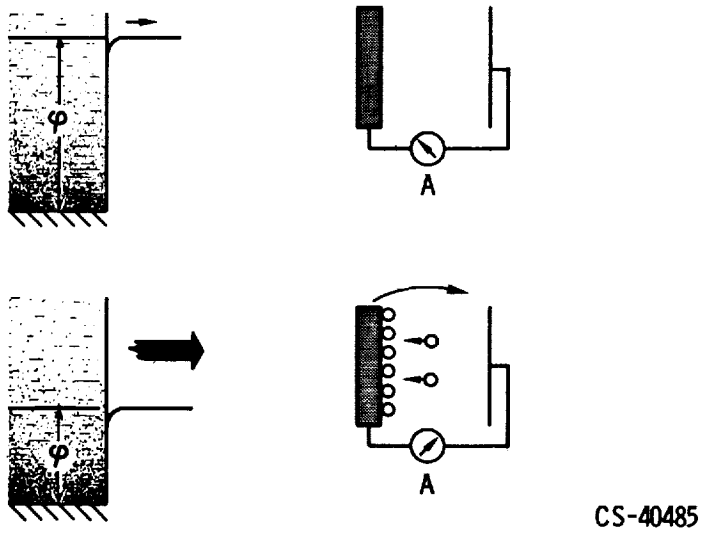

Figure IX-8. - Removal of electrons from emitter.

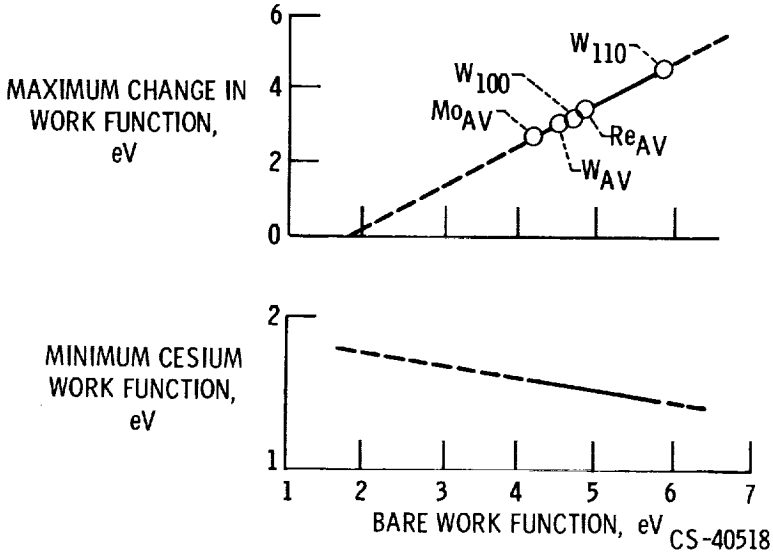

Figure IX-9. - Experimental work function correlation of bare and cesiated surfaces. (From Field Emission Corp.)

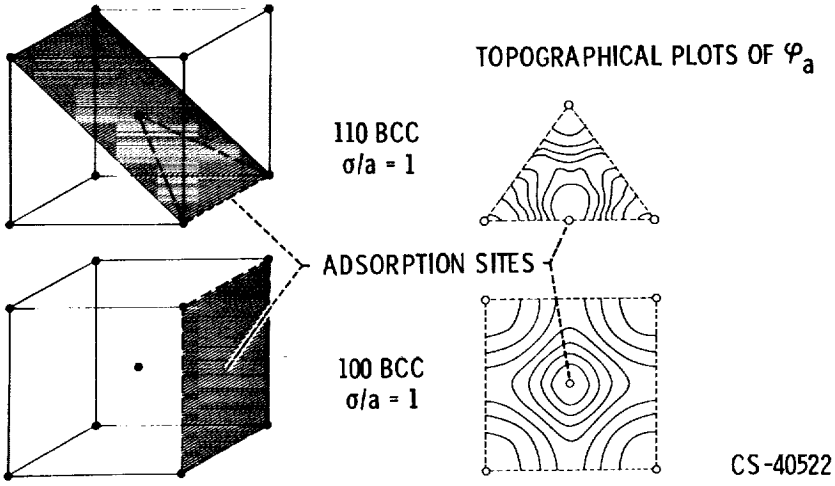

Figure IX-10. - Nature of ideal surface.

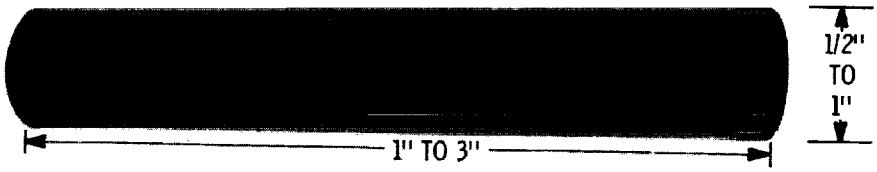

(a) Typical fuel containment cylinder.

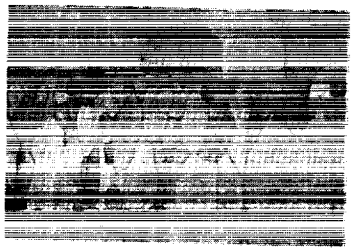

(b) Tungsten from hydrogen reduction of WCl_6. Approximately 110 plane.

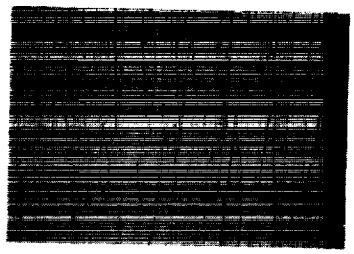

CS-40523

(c) Tungsten from hydrogen reduction of WF_6. Approximately 110 plane.

Figure IX-11. - Vapor-deposited tungsten emitters.

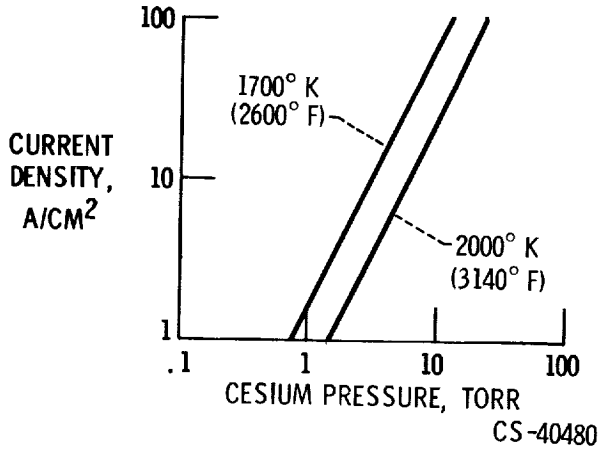

Figure IX-12. - Effect of cesium pressure on electron emission (based on data from diode using 110 oriented tungsten emitter).

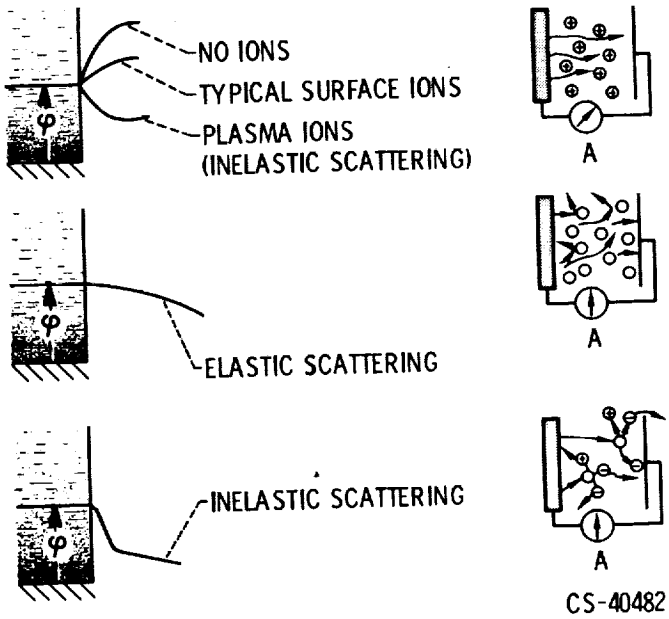

Figure IX-13. - Moving electrons across interelectrode space.

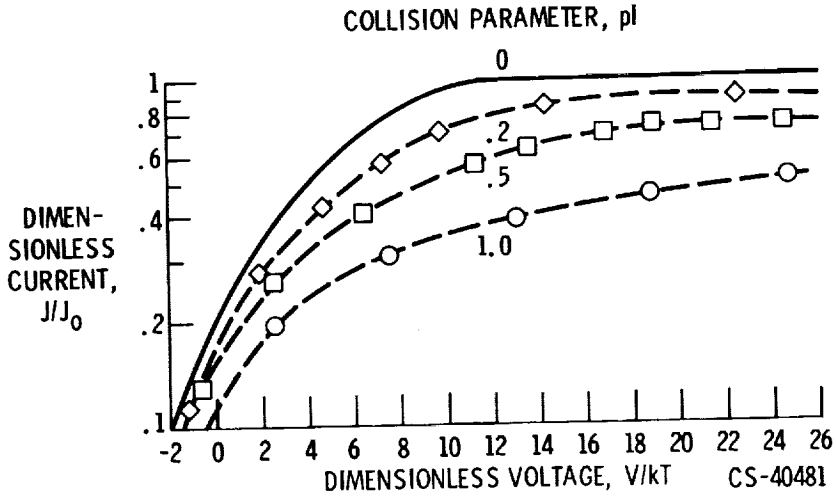

Figure IX-14. - Effect of argon on transmission of electrons in planar diode (including angular and velocity dependent elastic cross section).

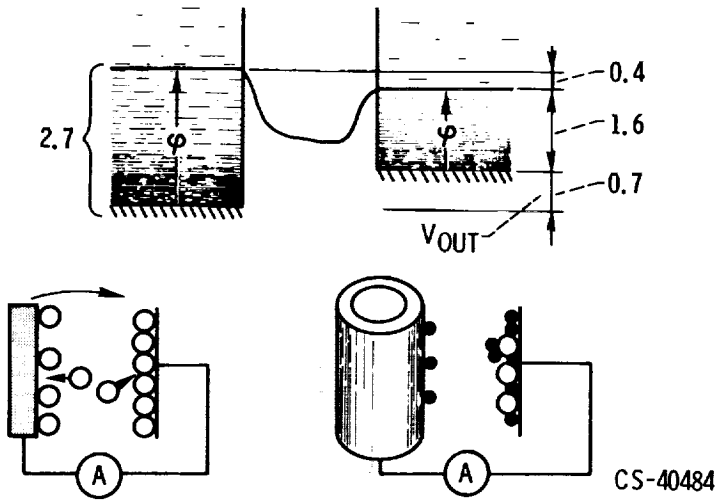

Figure IX-15. - Moving electrons into collector.

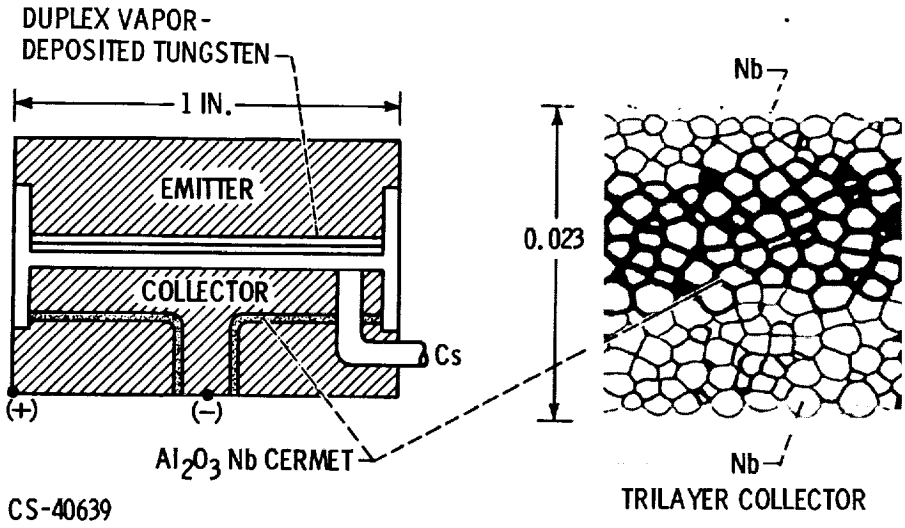

Figure IX-16. - Research converter.

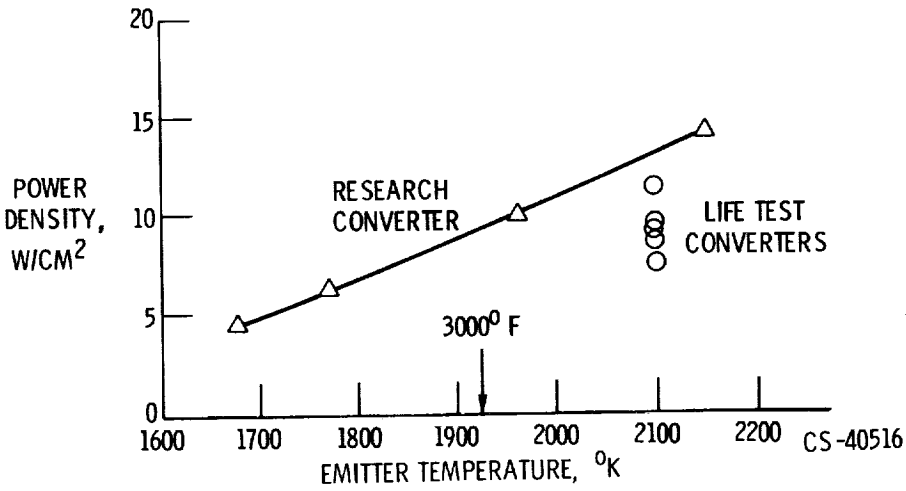

Figure IX-17. - Thermionic converter performance for electrically heated tungsten emitters. (From General Electric.)

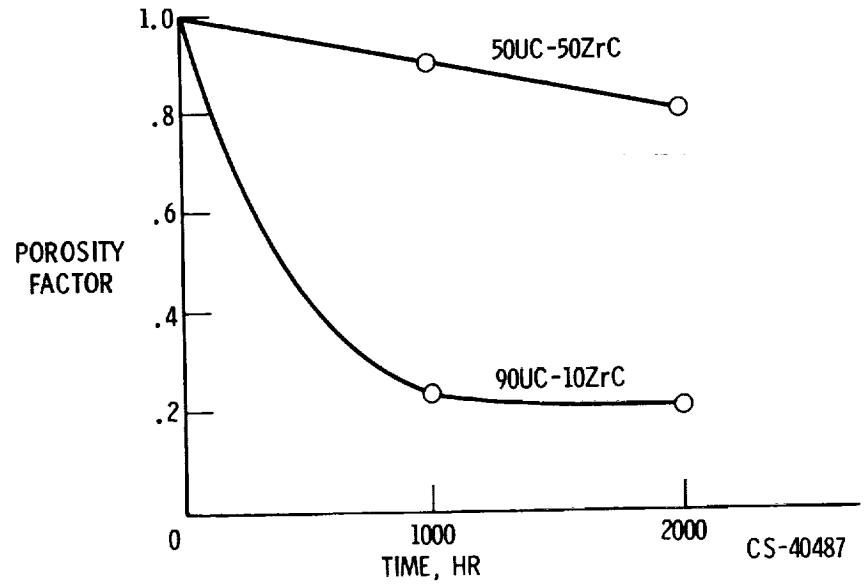

Figure IX-18. - Variation of uranium carbide - zirconium carbide porosity at 2100° K (3320° F). Isostatically cold pressed at 90 000 pounds per square inch; sintered 15 hours at 2300° K (3680° F). (From General Atomic.)

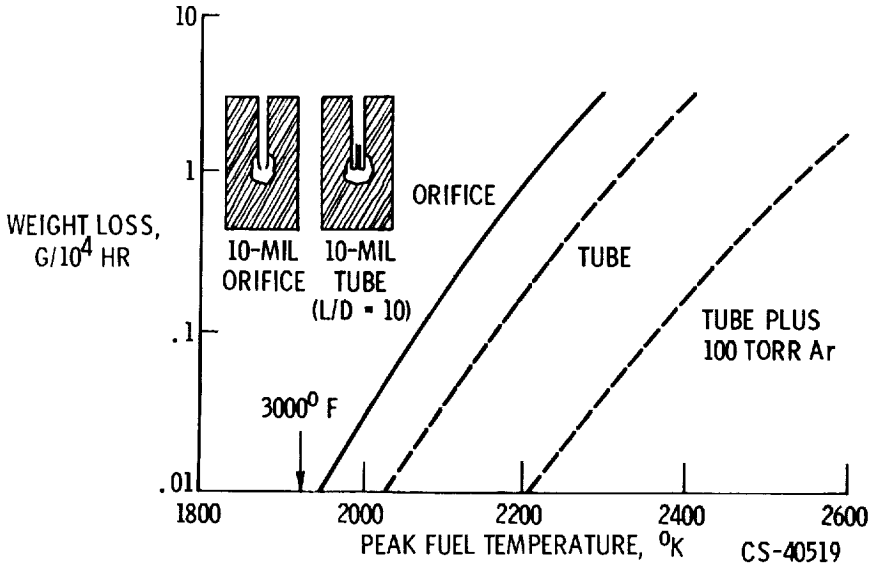

Figure IX-19. - Uranium dioxide vapor loss in vented fuel capsules.

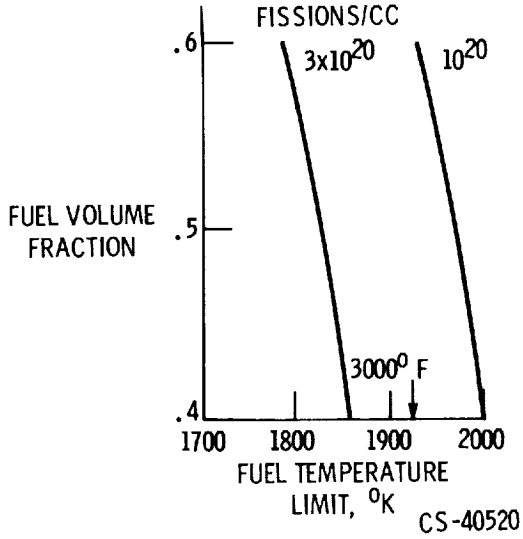

Figure IX-20. - Fuel volume fraction for uranium dioxide - tungsten cermet.
1 Percent creep for tungsten in 10^4 hours;
5 percent fission gas release at 1800° K;
50 percent fission gas release at 1900° K.

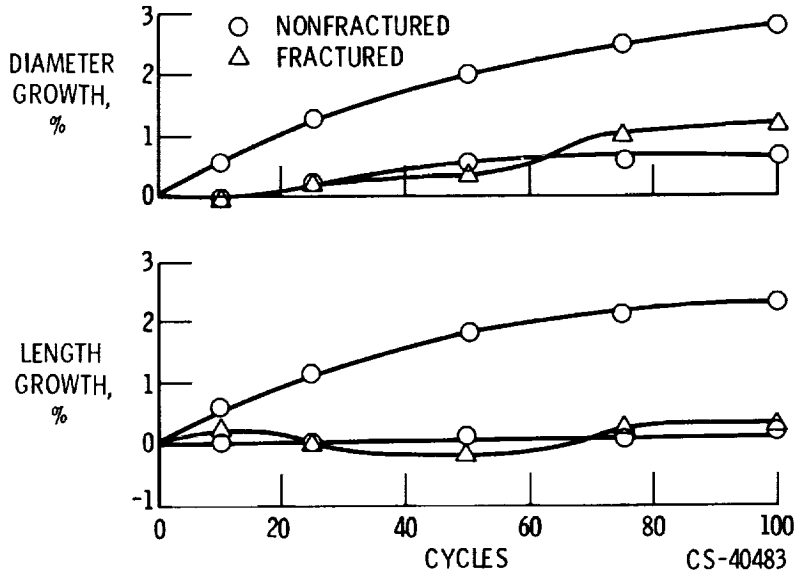

Figure IX-21. - Growth for thermal cycle specimens.